Benchmark full configuration interaction and equation-of-motion coupled-cluster model with single and double substitutions for ionized systems results for prototypical charge transfer systems: Noncovalent ionized dimers

Piotr A. Pieniazek
Department of Chemistry, University of Southern California, Los Angeles, California 90089-0482, USA

Stephen A. Arnstein
Center for Computational Molecular Science and Technology, School of Chemistry and Biochemistry, Georgia Institute of Technology, Atlanta, Georgia 30332-0400, USA

Stephen E. Bradforth and Anna I. Krylov[a)]
Department of Chemistry, University of Southern California, Los Angeles, California 90089-0482, USA

C. David Sherrill[b)]
Center for Computational Molecular Science and Technology, School of Chemistry and Biochemistry, Georgia Institute of Technology, Atlanta, Georgia 30332-0400, USA

(Received 2 July 2007; accepted 17 September 2007; published online 26 October 2007)

Benchmark full configuration interaction and equation-of-motion coupled-cluster model with single and double substitutions for ionized systems (EOM-IP-CCSD) results are presented for prototypical charge transfer species. EOM-IP-CCSD describes these doublet systems based on the closed-shell reference and thus avoids the doublet instability problem. The studied quantities are associated with the quality of the potential energy surface (PES) along the charge transfer coordinate and distribution of the charge between fragments. It is found that EOM-IP-CCSD is capable of describing accurately both the charge-localized and charge-delocalized systems, yielding accurate charge distributions and energies. This is in stark contrast with the methods based on the open-shell reference, which overlocalize the charge and produce a PES cusp when the fragments are indistinguishable. © *2007 American Institute of Physics*. [DOI: 10.1063/1.2795709]

I. INTRODUCTION

Ionized noncovalent dimers are relevant in electron/hole transfer (E/HT) processes ubiquitous in biophysics and molecular electronics,[1–4] and are described by open-shell doublet wave functions. Solvents used in radioactive element separation are susceptible to radiation induced ionization, which in the case of neat aromatic liquids leads to the initial formation of aromatic cations and dimer cations such as $(C_6H_6)_2^+$ and $(C_5H_5N)_2^+$.[5–8] Knowledge of the cation potential energy surface (PES) is needed in the interpretation of photoelectron spectra of neutral dimer species.[9–11] $(O_2)_2^+$ is an intermediate in the formation of protonated water clusters in the lower ionosphere.[12–14] Cation dimers of polyaromatic hydrocarbons are suspected to be the source of broad extended interstellar emission.[15] However, even in the case of simple isolated systems, such as $(O_2)_2^+$, $(CO_2)_2^+$, $(C_6H_6)_2^+$, and $(H_2O)_2^+$, the structure and properties have long eluded both theorists and experimentalists alike.[8,16–21]

For condensed phase problems Marcus theory[22–24] provides the relationship between the kinetics of the E/HT transfer processes and the electronic coupling between localized donor and acceptor sites. Often donor or acceptor sites are made up of dimer or multimeric cores, for example, the special pair of bacteriochlorophylls which serves as the electron donor in the photosynthetic reaction center.[25,26] In cytochrome *c* of bacterium *Schewanella oneidensis* MR-1 several heme groups acting concertedly are implicated in the reduction process, and, consequently, make the electron transfer (ET) process more efficient. This efficiency, referred to as "electron harvesting," has been attributed to the closely packed arrangement of the heme groups.[27,28] Oxidative damage on DNA leads to facile hole transfer between stacked aromatic bases.[29]

To explain and understand the function of these important biological systems, as well as to engineer compounds, one must obtain knowledge of the energetics and properties of the states involved. Especially vital is the value of the diabatic coupling between the donor and acceptor moieties, which should be calculated with an accuracy independent of relative orientations and distance between the two.

Several problems arise in approximate electronic structure calculations of doublet systems. Single-reference approaches based on an open-shell doublet reference are plagued by symmetry breaking,[30,31] even when highly correlated wave functions are used. Typically, the initial and final states involved in the hole/electron transfer process are nearly degenerate, and the wave functions acquire a considerable multideterminantal character. To this end multireference (MR) approaches have been used;[32–34] however, artifi-

[a)]Electronic mail: krylov@usc.edu
[b)]Electronic mail: sherrill@chemistry.gatech.edu

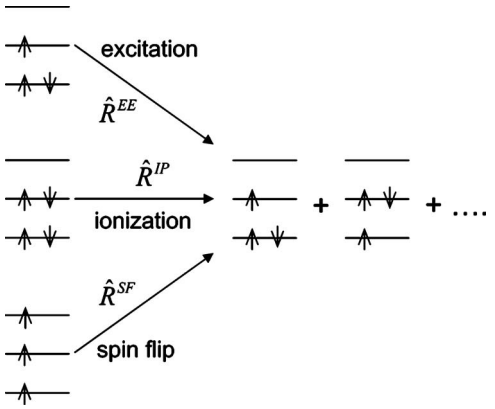

FIG. 1. Open-shell doublet wave functions can be described by several EOM approaches using different references/excitation operators. The EOM-IP method employs a well-behaved closed-shell reference.

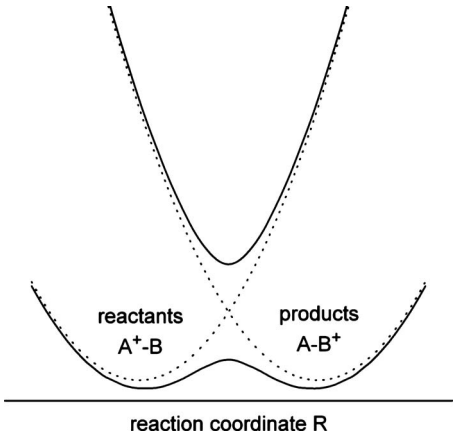

FIG. 2. Diabatic (dashed line) and adiabatic potential energy surfaces for electron transfer reactions. Diabatic states correspond to reactant and product electronic wave functions, i.e., the charge fully localized on one of the species, while adiabatic states are eigenfunctions of the electronic Hamiltonian. Marcus theory relates the coupling between diabatic states to the rate of electron/hole transfer process.

cial symmetry breaking can occur for MR wave functions as well.[35] Moreover, it requires the choice of an active space and may lead to unbalanced description of electronic states along the charge transfer (CT) path. Recently, the spin-flip (SF) approach[36–38] based on the quartet reference has been tested.[39] Although SF wave functions include all the leading electronic configurations, the quartet reference exhibits instability, which affects the quality of the PES.

The symmetry breaking problem is most readily manifested in the case of open-shell symmetric dimers, i.e., when the donor and acceptor moieties are indistinguishable. In this case, there are two Hartree-Fock (HF) solutions: the delocalized wave function, which has a correct symmetry, and a lower-energy symmetry-broken one. The energetic difference persists even at correlated levels of theory and vanishes only in the full configuration interaction (FCI) limit, where the correct symmetry is restored. For example, in the case of the ethylene dimer cation studied herein the difference between the symmetric and symmetry-broken HF solutions is 0.2 eV. One thus faces a dilemma of which solution to choose.[40] The symmetric, charge-delocalized solution has the correct symmetry at the symmetric nuclear configuration, but it may not be the best solution in a variational sense. On the other hand, the lower-energy solution does not exhibit the proper symmetry of the molecule at the symmetric nuclear configuration, and can therefore exhibit unphysical properties (such as artificially nonzero dipole moments). Moreover, from a practical point of view, the presence of these two different solutions can cause severe difficulties. Straightforward application of electronic structure programs will typically lead to the lower-energy, symmetry-broken solution being found at nonsymmetric geometries, and the higher-energy, symmetric solution being found at the symmetric geometry. This would lead to an undesirable and artificial discontinuity in the potential energy surface. Vibrational frequencies can be adversely affected no matter which solution is chosen.[41]

CT systems also pose challenges to density functional theory (DFT) due to self-interaction error (SIE), of which the H_2^+ dissociation curve is the most striking example.[42] SIE, which is present in many functionals, causes artificial stabilization of delocalized charge,[43–45] which spoils the description of Rydberg and CT excited states (see, for example, Refs. 46 and 47), vibronic interactions,[48,49] and charge distribution in the ground-state CT systems.[45]

This work presents FCI calculations of PESs and properties and demonstrates how to alleviate the problems mentioned above using single-reference equation-of-motion coupled-cluster model for ionized systems (EOM-IP-CC) methodology. A suitable reference in this case is the neutral HF wave function, which does not suffer from the instability problems as all the electrons are paired, and the target ionic wave functions are derived by removing an electron from the reference. Implementation of this Koopmans-like idea within coupled-cluster (CC) framework is the essence of the EOM-IP-CC method.[50–55] This method has been applied earlier by Yang and Hsu to a series of alkyl compounds and ethylene dimer, but no extensive testing was performed.[56] A similar approach, albeit based on the truncated configuration interaction (CI) method, has been developed by Simons and Smith for the calculation of ionization energies and electron affinities.[57] Similar ideas are exploited by related symmetry-adapted cluster CI family of methods.[58,59]

Here, EOM-IP-CCSD and FCI results for open-shell dimer cation species are compared. To the best of our knowledge there are no previous full CI benchmarks analyzing symmetry breaking in radical cations of van der Waals dimers. The evaluated quantities pertain to charge transfer states, i.e., charge localized on either fragment. We compute the absolute energy, permanent dipole, transition dipole and electronic coupling. The coupling is evaluated using the generalized Mulliken-Hush[33,60] (GMH) model. Instead of the permanent dipole, which is origin dependent for a charged system, we report the charge on the more positive molecule. This is also a measure of the weight of a particular diabatic (defined as a charge-localized state) state in the wave function

$$q_A = \langle a\Psi_{A^+B} + b\Psi_{AB^+}|\hat{q_A}|a\Psi_{A^+B} + b\Psi_{AB^+}\rangle = |a|^2, \qquad (1)$$

where q_A is the charge on fragment A and $\hat{q}_A$ is the associated operator.

TABLE I. Total energy (hartree), energy splitting (cm^{-1}) between Σ_u^+ and Σ_g^+ states, and the transition dipole moment (a.u.) for He_2^+ calculated by EOM-IP-CCSD.

	2.50 Å	3.00 Å	4.00 Å	5.00 Å	6.00 Å
			cc-pVDZ		
E (hartree)	−4.888 182 1	−4.883 253 5	−4.881 353 1	−4.881 238 6	−4.881 227 5
ΔE (cm^{-1})	2929.0	824.5	38.73	0.585	0.0026
μ_{tr}	2.348	2.825	3.774	4.721	5.667
			aug-cc-pVDZ		
E (hartree)	−4.892 363 3	−4.886 841 2	−4.884 308 1	−4.884 011 7	−4.883 951 7
ΔE (cm^{-1})	3182.2	990.3	83.2	8.73	0.83
μ_{tr}	2.306	2.795	3.758	4.711	5.660
			cc-pVTZ		
E (hartree)	−4.906 600 4	−4.901 553 3	−4.899 418 9	−4.899 201 6	−4.899 172 1
ΔE (cm^{-1})	3023.5	915.9	74.78	4.30	0.12
μ_{tr}	2.332	2.815	3.769	4.718	5.664
			aug-cc-pVTZ		
E (hartree)	−4.907 799 4	−4.902 352 8	−4.899 913 6	−4.899 613 1	−4.899 557 7
ΔE (cm^{-1})	3125.9	966.7	87.4	7.01	0.70
μ_{tr}	2.307	2.796	3.758	4.711	5.660
			d-aug-cc-pVTZ		
E (hartree)	−4.907 823 0	−4.902 371 3	−4.899 932 8	−4.899 626 5	−4.899 569 1
ΔE (cm^{-1})	3125.1	966.3	87.9	7.33	0.74
μ_{tr}	2.307	2.796	3.758	4.711	5.660
			aug-cc-pVQZ		
E (hartree)	−4.910 609 3	−4.905 166 0	−4.902 739 8	−4.902 440 0	−4.902 380 8
ΔE (cm^{-1})	3117.8	962.8	87.45	7.41	−0.60
μ_{tr}	2.307	2.796	3.758	4.711	5.660
			aug-cc-pV5Z		
E (hartree)	−4.911 411 0	−4.905 961 1	−4.903 538 3	−4.903 239 4	−4.903 182 6
ΔE (cm^{-1})	3115.2	960.8	87.30	7.59	0.60
μ_{tr}	2.307	2.796	3.758	4.711	5.660

The structure of the paper is as follows. The next section describes theoretical methods (EOM-CC approach to open-shell doublet wave functions and generalized Mulliken-Hush diabatization scheme) and computational details. Results for the selected benchmark systems are given in Sec. III. The studied systems are He_2^+, $(H_2)_2^+$, $(BH\text{-}H_2)^+$, $(Be\text{-}BH)^+$, and $(LiH)_2^+$. They were chosen based on the feasibility of FCI calculations and the difference of IEs. Finally, the EOM-IP-CCSD methodology is applied to the ethylene dimer, an often studied model system for polymer conduction and π interactions.[32,39,56,61,62] Additional information is available through the EPAPS document.[63] Our final remarks are given in Sec. IV.

II. METHODOLOGY

A. EOM-CC approach to open-shell and electronically excited species

The EOM approach[37,64–69] allows one to describe many multiconfigurational wave functions within a single-reference formalism.[38,70,71] Conceptually, EOM is similar to CI: target EOM states are found by diagonalizing the so-called similarity transformed Hamiltonian $\bar{H} \equiv e^{-T} H e^{T}$ as follows:

$$\bar{H} R = E R, \tag{2}$$

where T and R are general excitation operators with respect to the reference determinant $|\Phi_0\rangle$. Operator T describes the dynamical correlation, while R allows one to access a variety of multideterminantal target states. Regardless of the choice of T, the spectrum of $\bar{H}$ is exactly the same as that of the original Hamiltonian H. Thus, in the limit of the complete many-electron basis set, EOM is identical to FCI. In a more practical case of a truncated basis, e.g., when T and R are truncated at single and double excitations, the EOM models are numerically superior to the corresponding CI models,[72] because correlation effects are "folded in" in the transformed Hamiltonian, while the computational scaling remains the same. Moreover, the truncated EOM models are rigorously size consistent (or, more precisely, size intensive)[73–78] provided that the amplitudes T satisfy the CC equations for the reference state $|\Phi_0\rangle$ and are truncated at sufficiently high level of excitation consistent with that of R as follows:

TABLE II. Total energy (hartree), energy splitting (cm^{-1}) between Σ_u^+ and Σ_g^+ states, and the transition dipole moment (a.u.) for He_2^+ calculated by FCI.

	2.50 Å	3.00 Å	4.00 Å	5.00 Å	6.00 Å
			cc-pVDZ		
E (hartree)	−4.888 214 8	−4.883 262 1	−4.881 353 6	−4.881 238 6	−4.881 227 4
ΔE (cm^{-1})	2939.5	827.5	38.85	0.587	0.0027
μ_{tr}	2.347	2.825	3.774	4.721	5.667
			aug-cc-pVDZ		
E (hartree)	−4.892 611 4	−4.886 956 6	−4.884 336 2	−4.884 021 8	−4.883 956 3
ΔE (cm^{-1})	3219.8	1005.9	85.25	9.04	0.87
μ_{tr}	2.298	2.790	3.755	4.709	5.659
			cc-pVTZ		
E (hartree)	−4.906 681 9	−4.901 584 3	−4.899 424 8	−4.899 203 5	−4.899 172 9
ΔE (cm^{-1})	3039.7	921.6	75.27	4.33	0.12
μ_{tr}	2.330	2.814	3.768	4.717	5.664
			aug-cc-pVTZ		
E (hartree)	−4.908 057 2	−4.902 476 2	−4.899 944 3	−4.899 624 2	−4.899 563 1
ΔE (cm^{-1})	3160.6	981.0	89.02	7.15	0.72
μ_{tr}	2.299	2.790	3.755	4.709	5.658
			d-aug-cc-pVTZ		
E (hartree)	−4.908 081 5	−4.902 496 4	−4.899 965 2	−4.899 638 1	−4.899 574 4
ΔE (cm^{-1})	3159.7	980.9	89.78	7.55	0.77
μ_{tr}	2.299	2.790	3.755	4.709	5.658
			aug-cc-pVQZ		
E (hartree)	−4.910 866 5	−4.905 289 7	−4.902 771 6	−4.902 451 4	−4.902 388 9
ΔE (cm^{-1})	3150.8	976.6	89.17	7.58	0.62
μ_{tr}	2.299	2.790	3.755	4.709	5.658
			aug-cc-pV5Z		
E (hartree)	−4.911 666 4	−4.906 084 0	−4.903 570 3	−4.903 251 0	−4.903 187 8
ΔE (cm^{-1})	3147.5	974.3	89.04	7.77	0.62
μ_{tr}	2.299	2.790	3.755	4.709	5.658

$$\langle \Phi_\mu | \bar{H} | \Phi_0 \rangle, \tag{3}$$

where Φ_μ denotes μ-tuply excited determinants, e.g., $\{\Phi_i^a, \Phi_{ij}^{ab}\}$ in the case of CCSD.

By combining different types of excitation operators and references $|\Phi_0\rangle$, open-shell doublet states can be accessed in different ways, as explained in Fig. 1. For example, we may use the open-shell doublet reference and operators R that conserve the number of electrons and a total spin.[66,68,73] In this case, one CT state will be described at the CC level, while the other one at the equation-of-motion coupled-cluster for excitation energies (EOM-EE-CC) level. Problems arise due to the instability of the reference and unbalanced description of the two states. Inclusion of higher excitations, e.g., within EOM-CCSDT or EOM-CCSDt schemes[79,80] will of course improve the description, but at the price of increased computational costs.

The ionized/electron attached EOM models,[50–52,54,55,81] which employ operators R that are not electron conserving (i.e., include different number of creation and annihilation operators), describe ground and excited states of doublet radicals on equal footing. In our case, we start with a neutral reference and treat both CT states as ionized states. The truncation of EOM-IP operators deserves additional comments. For CCSD references, i.e., when operator T includes single and double excitations, the most common strategy is to retain only $1h$ and $2h1p$ operators as follows:

$$R^{\mathrm{IP}} = \sum r_i i + \sum r_{ij}^a a^+ ji, \tag{4}$$

which gives rise to the EOM-IP-CCSD method. However, one may consider including $3h2p$ operators as well, as in EOM-IP-CC(2,3).[82,83] As demonstrated by Piecuch and Bartlett, this does not break the size consistency of the resulting EOM-IP method,[84] in contrast to EOM-EE,[85] thus justifying such truncation scheme.

Finally, the EOM-SF method,[36–38] in which the excitation operators include spin flip, allows one to access diradicals, triradicals, and bond breaking without using spin- and symmetry-broken unrestricted HF (UHF) references. In our cases quartet reference would be used, as first proposed by You *et al.*[39] The obtained set of determinants is appropriate for the description of CT states, but the reference still exhibits its instability.

To summarize, the EOM-IP method avoids the HF instability problems and describes problematic open-shell doublet states in a single-reference formalism.

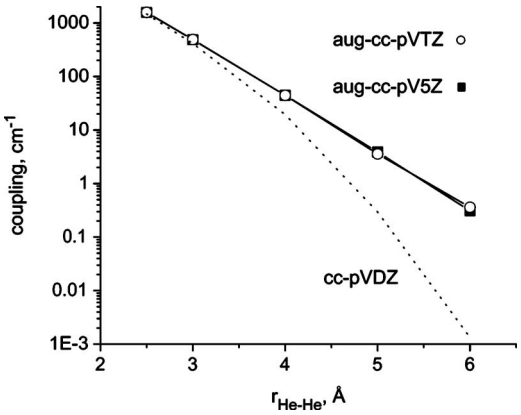

FIG. 3. Electronic coupling in the helium dimer as a function of distance using FCI.

B. Generalized Mulliken-Hush model

Figure 2 presents the PESs along the CT reaction coordinate. The solid lines represent the adiabatic energies, i.e., the eigenvalues of the electronic Hamiltonian. The dotted lines are the diabatic energies. The corresponding wave functions depend only weakly on nuclear configuration and describe the charge-localized states, i.e., A^+B and AB^+. The magnitude of the electronic coupling between these wave functions determines the kinetics of the process within the Marcus theory. Note that electronic structure packages yield *adiabatic* energies and wave functions.

The transformation between the two basis sets is not straightforward because diabatic states are not rigorously defined in a general case.[86] We employed the GMH method developed by Cave and Newton to compute the diabatic-adiabatic transformation matrix and the coupling elements. The method is based on the assumption that there is no dipole moment coupling between the diabatic states, and thus the dipole moment matrix is diagonal in this representation. This corresponds to the two states with the largest charge separation, i.e. charge localized on the reactants and products. The so-defined transformation matrix can hence be applied to the Hamiltonian matrix in the adiabatic representation yielding the coupling as the off-diagonal element. This leads to the following expression:

$$h_{ab} = \frac{\mu_{12}\Delta E_{ab}}{\Delta \mu_{ab}} = \frac{\mu_{12}\Delta E_{12}}{[(\Delta \mu_{12})^2 + 4(\mu_{12})^2]^{1/2}}. \tag{5}$$

The letter and number subscripts refer to diabatic and adiabatic quantities, respectively. μ_{12} is the transition dipole moment and $\Delta\mu_{12}$ is the difference between the permanent dipole moments. Components of each vector in the direction defined by the permanent dipole difference vector for the initial and final adiabatic states are used. In the case of a charged system the definition of the dipole moment depends on the origin. However, the diagonalization matrix depends on the *difference* rather than the values itself and thus is origin independent.

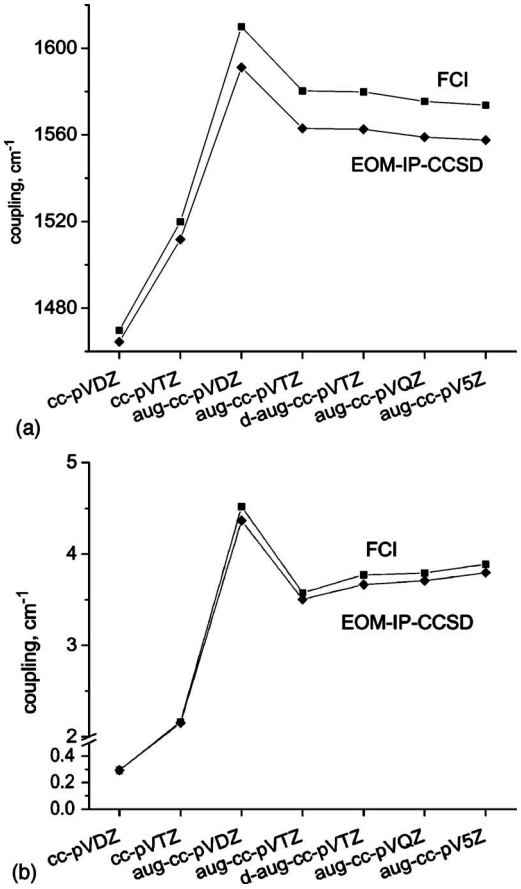

FIG. 4. Electronic coupling in He_2^+ at 2.5 (a) and 5.0 Å (b) calculated by FCI (squares) and EOM-IP-CCSD (diamonds).

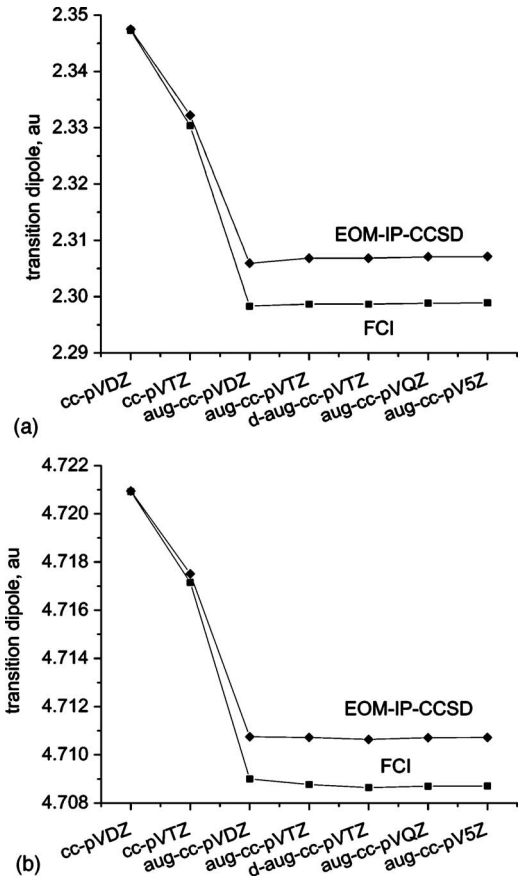

FIG. 5. The transition dipole moment in He_2^+ at 2.5 (a) and 5.0 Å (b) calculated by FCI (squares) and EOM-IP-CCSD (diamonds).

TABLE III. Total energy (hartree), energy splitting (cm^{-1}) between Σ_u^+ and Σ_g^+ states, and the transition dipole moment (a.u.) for He_2^+ using open-shell reference in aug-cc-pVTZ basis set.

	2.50 Å	3.00 Å	4.00 Å	5.00 Å	6.00 Å
HF/CIS			Spatial symmetry restricted UHF reference		
E (hartree)	−4.846 127 0	−4.840 118 4	−4.837 356 7	−4.837 024 9	−4.836 970 9
ΔE (cm^{-1})	−1105.15	−3569.53	−4623.83	−4724.96	−4732.74
μ_{tr}	2.297	2.781	3.735	4.680	5.622
HF/CIS			Broken spatial symmetry UHF reference		
E (hartree)	−4.861 965 5	−4.860 840 0	−4.860 314 2	−4.860 188 5	−4.860 144 8
ΔE (cm^{-1})	21 159.45	21 201.56	21 086.06	21 051.22	21 039.11
μ_{tr}	0.384	0.150	0.019	0.002	0.0003
q_{gr} (e)	0.019	0.008	0.003	0.002	0.001
q_{ex} (e)	1.025	0.994	0.996	0.998	0.999
CCSD/EOM-EE-CCSD			Spatial symmetry restricted UHF reference		
E (hartree)	−4.907 718 0	−4.902 132 0	−4.899 598 5	−4.899 278 6	−4.899 217 7
ΔE (cm^{-1})	3007.56	825.27	−66.65	−148.21	−154.48
μ_{tr}	2.299	2.790	3.755	4.709	5.659
CCSD/EOM-EE-CCSD			Broken spatial symmetry UHF reference		
E (hartree)	−4.906 403 3	−4.901 188 3	−4.899 750 8	−4.899 607 9	−4.899 561 4
ΔE (cm^{-1})	3185.51	1365.05	988.34	981.14	979.84
μ_{tr}	2.154	1.995	0.343	0.035	0.004
q_{gr} (e)	0.387	0.158	0.005	0.002	0.001
q_{ex} (e)	0.686	0.876	0.995	0.998	0.999

The main forte of the GMH model is its simplicity and a wide range of applicability. It can be applied both to the ground state and excited state at any nuclear configuration. Furthermore, the only required quantities are adiabatic, and thus easily available using standard electronic structure software.

Similar diabatization schemes exploiting differences in molecular properties of the diabatic states have been explored in other applications as well.[87–92]

C. The CT reaction coordinates

The two important coordinates for CT processes are the intermolecular separation and the intramolecular CT coordinate described below. In the charge transfer processes (Fig. 2) the reactants correspond to an electron/hole localized on one of the moieties, e.g., A^+-B. At infinite separation, the geometry of A is that of the cation, whereas the geometry of B is that of its neutral. The reaction corresponds to the positive charge moving from A to B and the nuclei rearranging such that A has the geometry of the neutral form and B has a cationlike geometry. At smaller interfragment separations, the geometries of the fragments along the reaction coordinate may differ from that simple picture. In principle, the geometries along this path can be calculated by following the energy minimum, i.e., conducting constrained optimization at each point along $A^+B \rightarrow AB^+$. Alternatively, a CT reaction coordinate can be approximated by arithmetic averaging of the Cartesian monomer coordinates

$$Q_{R1} = (1-R)Q_1 + RQ_2,$$
$$Q_{R2} = RQ_1 + (1-R)Q_2, \tag{6}$$

where Q_1 is the geometry of the neutral and Q_2 is the geometry of the cation. The averaging is done with the rotation axes and the centers of mass aligned. When $R=0$, A has its cation geometry, whereas B has its neutral geometry. At $R=0.5$ the geometry of each species is a simple average of the cation and neutral forms. Finally, at $R=1$ the geometry of A is that of the neutral, and that of B corresponds to the cation form. This approach merely ensures a smooth interpolation between the initial and final geometries and should not be taken as the path followed in a physical situation.

D. Computational details

Configuration interaction singles (CIS), EOM-IP-CCSD (IP-CCSD/$2h1p$), EOM-IP-CC(2,3) (IP-CCSD/$3h2p$), and EOM-CCSD for excitation energies (EOM-EE-CCSD) calculations as well as all geometry optimizations were performed using the QCHEM *ab initio* package.[93] FCI calculations employed the PSI3 package.[94] Multireference configuration interaction (MRCI) calculations were performed using MOLPRO.[95] All basis sets were obtained from the EMSL repository.[96]

The charge localized on the monomers was computed assuming that charges on individual fragments are point charges located at the c.m. of indivdual fragments. Only the component of the total dipole moment in this direction is considered. Charge q_A is localized on fragment A at position r_A, while charge $(1-q_A)$ is on fragment B localized at r_B. This yields the following expression for the charge:

TABLE IV. Total energy (hartree), energy splitting (cm^{-1}), transition dipole moment (a.u.), ground and excited state charge (a.u.), and coupling (cm^{-1}) calculated for $(H_2)_2^+$ at 3.0 Å separation in aug-cc-pVTZ basis set.

	0.0	0.2	0.4	0.45	0.5
			FCI		
E (hartree)	−1.779 004	−1.777 154	−1.771 929	−1.770 939	−1.770 563
ΔE (cm^{-1})	15 193	9720	5236	4601	4369
μ_{tr}	0.758	1.194	2.226	2.534	2.669
q_{gr} (e)	0.957	0.924	0.761	0.648	0.500
q_{ex} (e)	0.054 0	0.082 2	0.241	0.353	0.500
h_{ab} (cm^{-1})	2 156.2	2174.4	2183.5	2184.4	2184.7
			EOM-IP-CCSD		
E (hartree)	−1.778 861	−1.777 017	−1.771 813	−1.770 830	−1.770 456
ΔE (cm^{-1})	15 187	9723	5252	4620	4389
μ_{tr}	0.767	1.207	2.243	2.551	2.685
q_{gr} (e)	0.957	0.924	0.760	0.648	0.500
q_{ex} (e)	0.054 9	0.0831	0.242	0.354	0.500
h_{ab} (cm^{-1})	2 182.4	2196.5	2197.7	2195.7	2194.6
			EOM-EE-CCSD		
E (hartree)	−1.778 942	−1.777 015	−1.771 434	−1.770 244	−1.770 200
ΔE (cm^{-1})	15 891	10 303	5500	4695	4264
μ_{tr}	0.730	1.131	2.077	2.375	2.670
q_{gr} (e)	0.958	0.930	0.787	0.681	0.500
q_{ex} (e)	0.049 84	0.068 30	0.242 43	0.353 56	0.500
h_{ab} (cm^{-1})	2 167.3	2 165.3	2206.5	2186.6	2132.2

$$q_A = \frac{-\mu + r_B}{r_B - r_A}, \tag{7}$$

where the dipole moment vector μ is defined to point towards the positive charge. Vector quantities are computed relative to the c.m. of the system.

Spin-restricted references were used in EOM-IP-CC and FCI calculations. EOM-EE-CCSD calculations were based on spin-unrestricted references for H_2 dimer. Otherwise, spin-restricted open-shell references (ROHF) were employed. For the ethylene dimer, we considered both ROHF and UHF doublet references. CCSD energies were converged

TABLE V. Total energy (hartree), energy splitting (cm^{-1}), transition dipole moment (a.u.), ground and excited state charge (a.u.), and coupling (cm^{-1}) calculated for $(H_2)_2^+$ at 5.0 Å separation in aug-cc-pVTZ basis set.

	0.0	0.2	0.4	0.45	0.5
			FCI		
E (hartree)	−1.775 487	−1.772 451	−1.763 942	−1.761 042	−1.758 121
ΔE (cm^{-1})	14 882	8883	2956	1482	133.3
μ_{tr}	0.041 2	0.069 6	0.210	0.419	4.661
q_{gr} (e)	0.995	0.994	0.993	0.991	0.500
q_{ex} (e)	0.007 84	0.007 42	0.007 39	0.008 77	0.500
h_{ab} (cm^{-1})	65.76	66.33	66.60	66.63	66.64
			EOM-IP-CCSD		
E (hartree)	−1.775 475	−1.772 442	−1.763 936	−1.761 037	−1.757 504
ΔE (cm^{-1})	14 876	8880	2955	1482	135.9
μ_{tr}	0.042 2	0.071 2	0.215	0.428	4.667
q_{gr} (e)	0.995	0.994	0.993	0.991	0.500
q_{ex} (e)	0.008 07	0.007 58	0.007 51	0.008 94	0.500 00
h_{ab} (cm^{-1})	67.4	67.8	68.0	68.0	67.9
			EOM-EE-CCSD		
E (hartree)	−1.775 487	−1.772 451	−1.763 940	−1.761 038	−1.757 750
ΔE (cm^{-1})	15 630	9587	3620	2137	20.7
μ_{tr}	0.040	0.066	0.174	0.295	4.662
q_{gr} (e)	0.995	0.994	0.993	0.992	0.500
q_{ex} (e)	0.008 04	0.007 64	0.007 41	0.007 75	0.500
h_{ab} (cm^{-1})	66.9	67.4	67.6	67.5	10.3

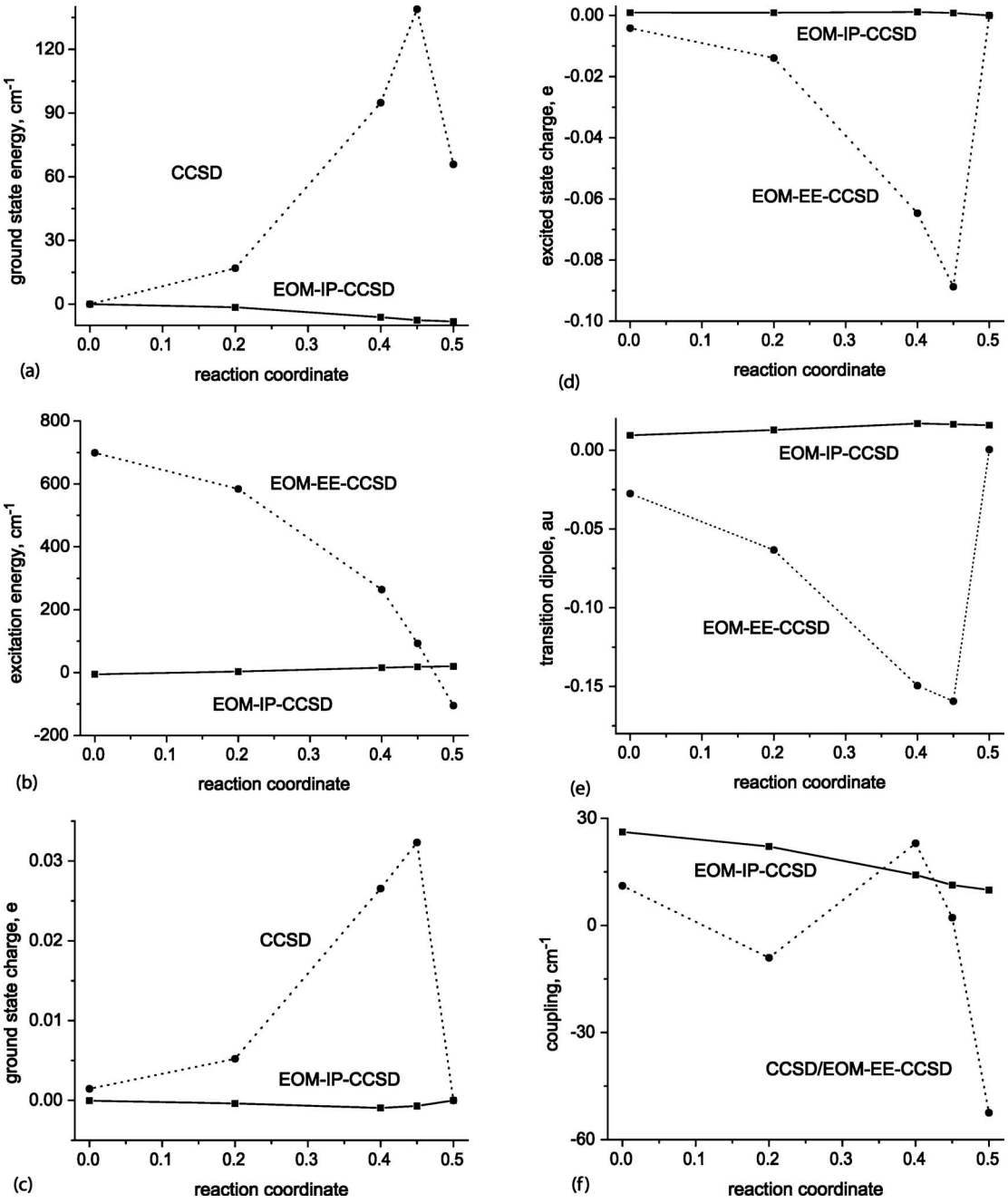

FIG. 6. Error in (a) ground state energy, (b) excitation energy, (c) ground state charge, (d) excited state charge, (e) transition dipole moment, and (f) diabatic coupling in $(H_2)^+$ dimer at 3.0 Å separation. EOM-IP-CCSD/aug-cc-pVTZ (solid line) and EOM-EE-CCSD/aug-cc-pVTZ (dotted line) results are shown.

to 10^{-10} hartree. Davidson iteration in EOM calculations were considered converged when the residue of the excited state vectors was below 10^{-10}. EOM-IP-CC(2,3) dipole moments for $(C_2H_4)_2^+$ were computed via finite differences using field values of ±0.000 01 a.u.

All electrons were active in EOM calculations. EOM dipole moments were calculated using fully relaxed one-particle density matrices, that is, including the amplitude and orbital response contributions,[97] while transition dipoles were computed as "expectation values," that is, using unrelaxed density matrices of the right-hand and left-hand eigenvectors.[68]

FCI properties were computed using unrelaxed density matrices. Orbital relaxation terms are not needed in FCI property computations because the FCI properties are invariant to unitary transformations of the active orbitals; the exception occurs when some orbitals are frozen in the correlated computation, as was the case here for the 1*s*-like orbitals for Be and B atoms. However, limited tests indicate that these core-active orbital rotations did not contribute significantly for the cases considered.

MRCI calculations employ the state-averaged complete active space self-consistent field (SA-CASSCF) reference and include all single and double excitations from the reference (MR-CISD).[98,99] To correct for the lack of size extensivity, the resulting MR-CISD energies are augmented by the Davidson correction[100] and are denoted as MR-CISD+Q. Unfortunately, no analog of the Davidson correction for

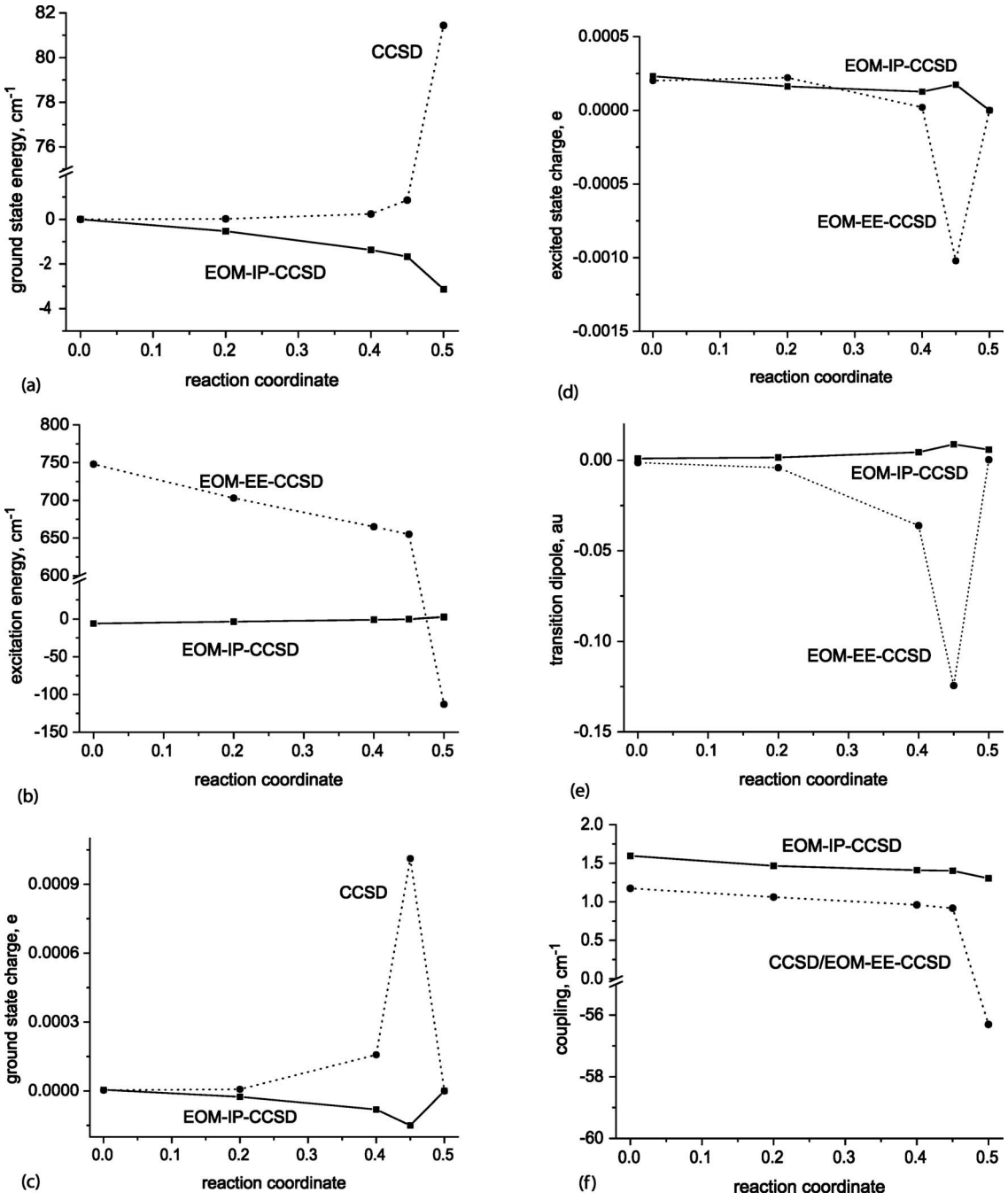

FIG. 7. Error in (a) ground state energy, (b) excitation energy, (c) ground state charge, (d) excited state charge, (e) transition dipole moment, and (f) diabatic coupling in $(H_2)^+$ at 5.0 Å separation. EOM-IP-CCSD/aug-cc-pVTZ (solid line) and EOM-EE-CCSD/aug-cc-pVTZ (dotted line) results are shown.

properties is available. The active space consisted of the ethylene π and π^* orbitals. The SA-CASSCF computations include the ground state and the first excited state with equal weights. The four $1s$ carbon orbitals were restricted in CASSCF calculations and frozen in MR-CISD.

Geometries of H_2, BH, and LiH were optimized using CCSD with perturbative account of triple excitations (CCSD(T)) (Refs. 101 and 102) and the aug-cc-pVTZ basis set. C_2H_4 and $C_2H_4^+$ structures were obtained using density functional theory (DFT) with B3LYP (Ref. 103) functional and the 6-311+G* basis set. All geometries are given in the EPAPS document.[63]

III. RESULTS AND DISCUSSION

A. $(He_2)^+$ dimer

Our first benchmark system is the helium dimer cation. Due to symmetry, the lower and upper charge transfer states, Σ_u^+ and Σ_g^+, feature the charge equally distributed between the helium atoms, and the coupling is simply half of the energy splitting between the two states. The energies and transition dipole moments were computed at intermolecular separations ranging from 2.5 to 6.0 Å. EOM-IP-CCSD and FCI results are presented in Tables I and II, respectively. Figure 3 shows the distance dependence of the FCI coupling. Only basis sets with diffuse functions reproduced the correct ex-

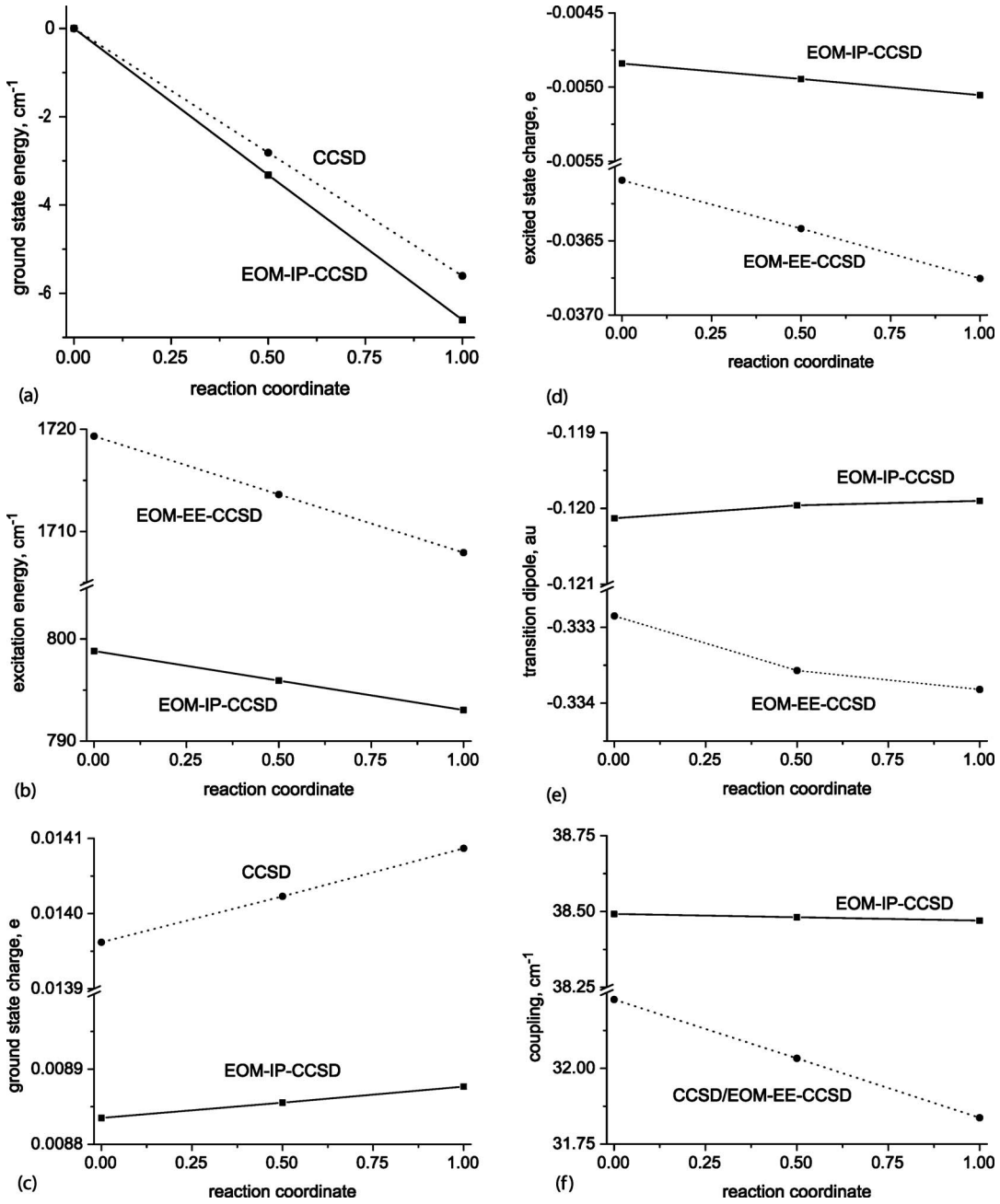

FIG. 8. Error in (a) ground state energy, (b) excitation energy, (c) ground state charge, (d) excited state charge, (e) transition dipole moment, and (f) diabatic coupling in $(Be–BH)^+$. EOM-IP-CCSD/aug-cc-pVDZ (solid line) and EOM-EE-CCSD/aug-cc-pVDZ (dotted line) results are shown. The charge pertains to the Be fragment.

ponential decay of the coupling. Without diffuse functions the coupling decays too fast. The magnitude of the coupling is nearly converged at the aug-cc-pVTZ basis.

The convergence of the coupling as a function of the method and the distance is shown in Fig. 4. The behavior of the two theoretical methods is essentially identical. Adding the first set of diffuse functions increases the coupling and the magnitude of this effect increases with distance. Further basis set expansion, e.g., adding another set of diffuse or valence functions, has smaller effects. The difference between double-ζ and triple-ζ is significant, but less important than the presence of diffuse functions. One aspect is very interesting—the error of the EOM-IP-CCSD versus FCI decreases at larger distances. We attribute this effect to larger dynamical correlation at shorter distances, i.e., when the distance between electrons is smaller on average. In He_2^+ at large separations, only two electrons need to be correlated for a good description dynamical correlation. A similar trend was observed in bond breaking applications of CASSCF and valence optimized orbital coupled cluster doubles methods.[104] Similar trends are observed for the transition dipole moment, as shown in Fig. 5. At least a single set of diffuse functions is needed and the values converge at the aug-cc-pVDZ basis set.

For this small benchmark system, we also investigated the performance of methods based on the doublet reference using the aug-cc-pVTZ basis set. These results are given in Table III. UHF-CIS gives qualitatively incorrect results, i.e.,

it places the excited state below the ground state, and the level splitting does not decay to zero at large distances. This behavior is not rectified by including electron correlation, even at the EOM-EE-CCSD level. The ordering is only correct at small distances; however, the asymptotic distance behavior is still lacking, which is quite unexpected for this three-electron system.

B. $(H_2)_2^+$ dimer

The hydrogen dimer cation is isoelectronic with He_2^+; however, due to the additional nuclear degree of freedom the molecular fragments no longer have to be identical, and the charge can be localized. From several possible orientations of the two fragments, we chose a C_{2v} symmetry configuration in which the two molecules are parallel. EOM-IP-CCSD, CCSD/EOM-EE-CCSD, and FCI calculations in the aug-cc-pVTZ basis were performed at reaction coordinate values of 0.0, 0.2, 0.4, 0.45, and 0.5 at 3.0 and 5.0 Å separations. The data are summarized in Tables IV and V and the error plots are given in Figs. 6 and 7. The EOM-IP-CCSD/aug-cc-pVTZ ionization energies (IEs) are 16.398 and 14.544 eV at neutral and cation geometries, respectively.

A brief explanation of the plots is in order. The errors are calculated as the difference between the approximate value and the exact FCI result. Negative values mean the given quantity is underestimated, while positive values mean the opposite. If the curve is parallel to the x axis, it means that the error is constant throughout the reaction coordinate space, a highly desirable feature. A slope, on the other hand, denotes a change in the quality of description and a nonparallelity error (NPE). The absolute values of the total energy are not important, and only NPEs are of interest—the error for the total energy of the ground state is arbitrarily set to 0 at $R=0$. For the ground state charge, if the error is positive it signifies that there is excessive charge separation, i.e., the state is overpolarized. Overpolarization of the excited state is manifested by a negative error.

Panels (a) and (b) in Figs. 6 and 7 show the error in the ground state total energy and excitation energy, respectively. At small values of R, i.e., when there is large difference between the geometries of the two fragments both methods perform similarly. As the bond lengths become more similar the discrepancy between EOM-EE-CCSD and FCI becomes more significant. Finally, at $R=0.5$ the doublet HF wave function becomes unstable yielding a cusp on the PES. It is manifested as a large jump on all the plots. Meanwhile the error for EOM-IP-CCSD curves remains small. At 5.0 Å separation and excluding the $R=0.5$ point, the EOM-EE-CCSD error in excitation energy ranges between 750 and 650 cm^{-1}. The EOM-IP-CCSD error is confined to the 6–0 cm^{-1} range. Similar behavior is observed at 3.0 Å separation. In other words, the EOM-EE-CCSD NPE is high and the description is not uniform throughout the reaction coordinate space.

An important property of a CT system is its charge distribution. Panels (c) and (d) of Figs. 6 and 7 show the ground and excited state charge of the more positively charged fragment (in the ground state) at the two interfragment separations. In both cases the EOM-IP-CCSD and FCI results are essentially identical, and the NPE is small. The quality of CCSD/EOM-EE-CCSD description degrades towards $R=0.5$. Both the ground and excited states become overpolarized as a consequence of the charge-localized character of the UHF doublet reference. The incorrect charge distribution in turn affects the transition dipole moment [Figs. 6(e) and 7(e)]. Again, the EOM-IP-CCSD description is uniform and accurate throughout, while EOM-EE-CCSD underestimates this property.

TABLE VI. Total energy (hartree), energy splitting (cm^{-1}), transition dipole moment (a.u.), ground and excited state charge (a.u.), and coupling (cm^{-1}) calculated for linear $(Be–BH)^+$ at 5.0 Å separation in aug-cc-pVDZ basis set. The charge pertains to the Be fragment.

	0.0	0.5	1.0
		FCI	
E (hartree)	−39.505 862	−39.505 843	−39.505 790
ΔE (cm^{-1})	5295.0	5282.9	5270.6
μ_{tr} (a.u.)	1.643	1.647	1.648
q_{gr} (e)	0.864 8	0.863 9	0.863 0
q_{ex} (e)	0.062 9	0.063 4	0.063 9
h_{ab} (cm^{-1})	1053.1	1053.8	1054.5
		EOM-IP-CCSD	
E (hartree)	−39.506 545	−39.506 542	−39.506 503
ΔE (cm^{-1})	5903.8	5889.0	5873.8
μ_{tr} (a.u.)	1.522	1.527	1.528
q_{gr} (e)	0.873 7	0.872 8	0.871 9
q_{ex} (e)	0.064 0	0.064 5	0.065 0
h_{ab} (cm^{-1})	1091.6	1092.3	1093.0
		EOM-EE-CCSD	
E (hartree)	−39.505 518	−39.505 513	−39.505 472
ΔE (cm^{-1})	6878.9	6861.8	6844.4
μ_{tr} (a.u.)	1.310	1.313	1.315
q_{gr} (e)	0.878 8	0.878 0	0.877 1
q_{ex} (e)	0.045 1	0.045 5	0.045 9
h_{ab} (cm^{-1})	1085.4	1085.9	1086.4

The calculated couplings depend on the energy splitting, transition, and permanent dipole moment of the two states. The values are plotted in panel (f) of Figs. 6 and 7. The most striking feature is the cusp of the EOM-EE-CCSD curve at the transition state. It originates from the CCSD PES cusp, as the coupling at this point is equal to half the energy splitting between the two states. EOM-IP-CCSD systematically overestimates the coupling, due to the error in the transition dipole. The coupling weakly depends on the reaction coordinate, in agreement with the Condon approximation, i.e., the coupling only depends on the molecular coordinates that do not affect the effective donor-acceptor distance.

C. $(Be–BH)^+$ dimer

The $(Be–BH)^+$ dimer cation was studied in a linear configuration, with the beryllium atom located on the boron side. aug-cc-pVDZ basis set was used in the calculations. The data are presented in Table VI and the error plots are shown in Fig. 8. The BH distance was scanned from its cation geometry ($R=0$) to the neutral geometry ($R=1$). The distance be-

TABLE VII. Total energy (hartree), energy splitting (cm^{-1}), transition dipole moment (a.u.), ground and excited state charge (a.u.), and coupling (cm^{-1}) calculated for t-shaped $(BH-H_2)^+$ at 3.0 Å separation in aug-cc-pVDZ basis set. The charge pertains to the BH fragment.

	0.0	0.25	0.5	0.75	1.0
			FCI		
E (hartree)	−26.030 624	−26.029 212	−26.022 318	−26.012 228	−26.000 430
ΔE (cm^{-1})	48 228	44 230	40 742	37 712	35 094
μ_{tr} (a.u.)	0.630 0	0.684 2	0.745 7	0.810 5	0.876 1
q_{gr} (e)	0.998	0.993	0.987	0.981	0.975
q_{ex} (e)	0.222	0.220	0.221	0.223	0.226
h_{ab} (cm^{-1})	6 643	6 592	6 612	6 652	6 694
			EOM-IP-CCSD		
E (hartree)	−26.028 457	−26.027 055	−26.020 179	−26.010 118	−25.998 359
ΔE (cm^{-1})	47 467	43 465	39 984	36 969	34 373
μ_{tr} (a.u.)	0.646 9	0.707 0	0.773 3	0.842 5	0.912 4
q_{gr} (e)	0.995	0.990	0.984	0.977	0.970
q_{ex} (e)	0.214	0.214	0.216	0.219	0.223
h_{ab} (cm^{-1})	6 654	6 651	6 692	6 745	6 797
			EOM-EE-CCSD		
E (hartree)	−26.030 734	−26.029 311	−26.022 403	−26.012 297	−26.000 479
ΔE (cm^{-1})	49 088	45 053	41 523	38 448	35 783
μ_{tr} (a.u.)	0.627 3	0.678 5	0.737 5	0.799 8	0.863 0
q_{gr} (e)	0.997	0.992	0.987	0.982	0.976
q_{ex} (e)	0.224	0.220	0.219	0.220	0.222
h_{ab} (cm^{-1})	6 754	6 669	6 663	6 679	6 695

tween the c.m. of both fragments was kept constant at 5.0 Å. EOM-IP-CCSD/aug-cc-pVDZ vertical IE of beryllium is 9.234 eV, while that of BH decreases from 9.687 to 9.679 eV as the bond length increases from the cation to the neutral geometry. The fact that the IE of BH at the cation geometry is larger than at the neutral geometry is due to the fact that the equilibrium bond lengths were optimized at a different level of theory. It is not a problem in other systems due to larger geometric change. Due to the small changes in the relative energies of both species only subtle changes are expected along the reaction coordinate. Before delving into the details note that both CCSD/EOM-EE-CCSD and EOM-IP-CCSD (in all cases except the ground state energy) capture the trends in properties along the reaction coordinate. The NPE is smaller for EOM-IP-CCSD indicating a more uniform description throughout the reaction coordinate space.

The IEs of both fragments are very close, thus we expect an appreciable extent of charge delocalization. In the ground state roughly 86% of the hole is located on Be, while only 6% in the excited state. Both EOM-IP-CCSD and CCSD predict a slightly more localized structure than FCI, in both states. This in turn affects the transition dipole moment, which decreases as follows: FCI > EOM-IP-CCSD > EOM-EE-CCSD. Clearly, the more charge localized the state is, the lower the transition dipole moment is. The inverse is true for the excitation energies: FCI values are lower than EOM-EE-CCSD, while EOM-IP-CCSD is in between. Lastly, let us look at the diabatic coupling, which is a cumulative property. Unexpectedly, all methods are in very good accord, within 5%. The agreement for EOM-IP is only slightly inferior than for EOM-EE-CCSD. This is very interesting, as both methods give slightly different picture of the states. In case of EOM-EE-CCSD, the increased transition energy is compensated by the decreased transition dipole. In the denominator the increased difference in permanent dipole moments compensates for the underestimated transition dipole, see Eq. (5).

D. $(BH-H_2)^+$ dimer

The $BH-H_2$ system is an example complementary to Be–BH. The difference in vertical ionization energies is approximately 6 eV, much larger than 0.5 eV in Be–BH. At the cation geometry, the EOM-IP-CCSD/aug-cc-pVDZ IEs of BH and H_2 are 9.687 and 14.460 eV, respectively; values at neutral geometries are 9.679 and 16.288 eV. We studied the system in a t-shaped configuration: the H_2 molecule constitutes the top, while BH (boron atom closer to H_2) is the stem. At $R=0$, H_2 is at its neutral geometry while BH is at its cation geometry. At $R=1$, BH is at its neutral geometry, while H_2 is at the cation geometry. The distance between c.m.'s is kept fixed at 3.0 Å. The data are listed in Table VII and error plots are given in Fig. 9. The aug-cc-pVDZ basis set was used in the calculations.

The performance of EOM-IP-CCSD and CCSD/EOM-EE-CCSD is very similar. The errors are smaller for the latter, but the difference is not significant compared to the quantities involved. For instance, at $R=0.5$ the former underestimates the excitation energy by 750 cm^{-1}, while the latter overestimates it by the same amount. The value of the excitation energy is ~40 000 cm^{-1} using all methods. With increased R the energy spacing decreases and CCSD/EOM-EE-CCSD tends to overpolarize both states while EOM-IP-

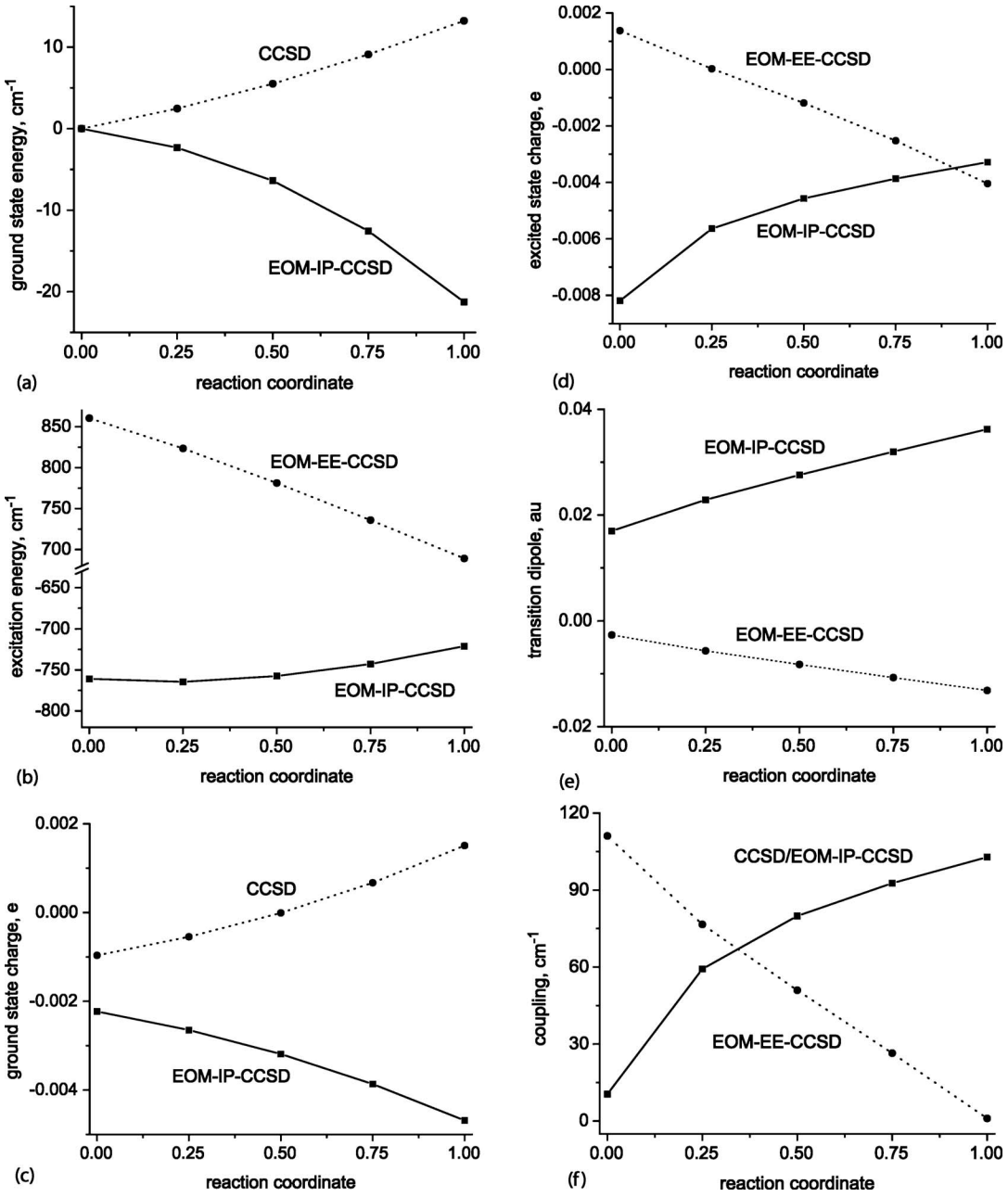

FIG. 9. Error in (a) ground state energy, (b) excitation energy, (c) ground state charge, (d) excited state charge, (e) transition dipole moment, and (f) diabatic coupling in $(BH-H_2)^+$. EOM-IP-CCSD/aug-cc-pVDZ (solid line) and EOM-EE-CCSD/aug-cc-pVDZ (dotted line) results are shown. The charge pertains to the BH fragment.

CCSD underpolarizes them. Nonetheless, all methods predict the hole to be almost entirely located on BH in the ground state, and on H_2 in the excited state. This is in agreement with the difference of IEs, and according to Eq. (1) signifies a very similar character of diabatic and adiabatic wave functions. Another way of understanding it is by comparing the diabatic coupling with the energy difference between the adiabatic levels. Consider a two-level coupled system. If the two levels are degenerate, they will split by twice the amount for the coupling. In the case, when they are nondegenerate, the amount of splitting induced by the coupling will be less than twice its value. Thus, in $(BH-H_2)^+$ dimer diabatic coupling can account for utmost 13 000 cm^{-1} of adiabatic state separation. The smallest difference between them occurs at $R=1$, and is equal to 35 000 cm^{-1}. The difference, 22 000 cm^{-1}, is the difference between energies of the diabatic states. Since it is significantly larger than the coupling, the adiabatic states will be very similar to the diabatic states. This is additionally confirmed by good agreement of transition dipoles between EOM-IP-CCSD and EOM-EE-CCSD. For this molecular system both methods perform similarly and other than the computational cost there is no preference for either one.

E. $(LiH)_2^+$ dimer

The LiH dimer cation cation was studied in a stacked antiparallel configuration. The separation between c.m. was

TABLE VIII. Total energy (hartree), energy splitting (cm^{-1}), transition dipole moment (a.u.), ground and excited state charge (a.u.), and coupling (cm^{-1}) calculated for $(LiH)_2^+$ at 4.0 Å separation in 6-31+G basis set.

	0.0	0.2	0.4	0.45	0.5
			FCI		
E (hartree)	−15.742 224 1	−15.742 885 3	−15.742 017 6	−15.741 853 6	−15.741 794 1
ΔE (cm^{-1})	6862.5	4924.4	3500.7	3333.3	3275.5
μ_{tr}	1.519	2.131	3.006	3.158	3.214
q_{gr} (e)	0.845	0.788	0.634	0.570	0.500
q_{ex} (e)	0.222	0.252	0.379	0.436	0.500
h_{ab} (cm^{-1})	1661.4	1646.9	1638.8	1638.0	1637.7
			EOM-IP-CCSD		
E (hartree)	−15.738 308 7	−15.738 352 9	−15.736 769 7	−15.736 488 8	−15.736 386 3
ΔE (cm^{-1})	7478.7	5141.0	3339.6	3115.0	3036.3
μ_{tr}	1.576	2.290	3.522	3.776	3.874
q_{gr} (e)	0.888	0.840	0.674	0.593	0.500
q_{ex} (e)	0.141	0.178	0.332	0.410	0.500
h_{ab} (cm^{-1})	1614.6	1584.3	1534.1	1522.7	1518.2

held fixed at 4.0 Å. The monomer state considered here corresponds to ionization from the σ bonding orbital of the monomer. According to EOM-IP-CCSD/6-31+G it requires 6.781 and 7.589 eV at the cation and neutral geometries, respectively. The data are listed in Table VIII and error plots are given in Fig. 10. The 6-31+G basis set was used in the calculations. The large difference between the IEs causes a significant change in the extent of charge delocalization along the reaction coordinate. This is in stark contrast to BH. Low coupling to Be or H_2 precluded the use of LiH in the heterodimer calculations.

Panels (a) and (b) of Fig. 10 present the error in the ground state total energy and the excitation energy, respectively. There is a significant NPE in both. EOM-IP-CCSD predicts a larger energy change when going from $R=0$ to $R=0.5$. At $R=0$ the excitation energy is overestimated by 600 cm^{-1}, while it is underestimated by 200 cm^{-1} at $R=0.5$. These numbers do not exceed 10%. FCI yields a less polarized state and a lower transition dipole moment. The error in the transition moment increases as the monomers become more similar. Lastly, EOM-IP-CCSD predicts weaker diabatic coupling than FCI. Note that the NPE is much smaller for the coupling than for the other quantities.

F. $(C_2H_4)_2^+$

The results in this section are obtained using 6-31+G basis set. Monomer geometries of ethylene are given in the EPAPS document.[63] The biggest difference between the neutral and the cation geometry is the C–C bond length: 1.418

TABLE IX. Total energy (hartree), energy splitting (cm^{-1}), transition dipole moment (a.u.), ground and excited state charge (a.u.), and coupling (cm^{-1}) calculated for $(C_2H_4)_2^+$ at 4.0 Å separation in 6-31+G basis set.

	0.0	0.2	0.4	0.45	0.5
			EOM-IP-CCSD		
E (hartree)	−156.078 063	−156.079 790	−156.080 620	−156.080 697	−156.080 723
ΔE (cm^{-1})	5239	4841	4630	4609	4603
μ_{tr} (a.u.)	3.142	3.404	3.561	3.577	3.582
q_{gr} (e)	0.733	0.652	0.553	0.527	0.500
q_{ex} (e)	0.277	0.355	0.450	0.475	0.500
h_{ab} (cm^{-1})	2303.8	2302.6	2301.4	2301.3	2301.3
			EOM-IP-CC(2,3)		
E (hartree)	156.083 897	−156.085 381	−156.086 074	−156.086 138	−156.086 159
ΔE (cm^{-1})	5447	4948	4680	4654	4646
q_{gr} (e)	0.747	0.663	0.557	0.529	0.500
q_{ex} (e)	0.256	0.339	0.443	0.471	0.500
			MR-CISD+Q		
E (hartree)	−156.077 664	−156.079 075	−156.079 722	−156.079 781	−156.079 716
ΔE (cm^{-1})	5352	4885	4636	4612	4610
μ_{tr}	3.215	3.456	3.597	3.611	3.621
q_{gr} (e)	0.722	0.643	0.550	0.525	0.500
q_{ex} (e)	0.285	0.362	0.452	0.476	0.500
h_{ab} (cm^{-1})	2393.4	2334.6	2305.8	2302.9	2305.2

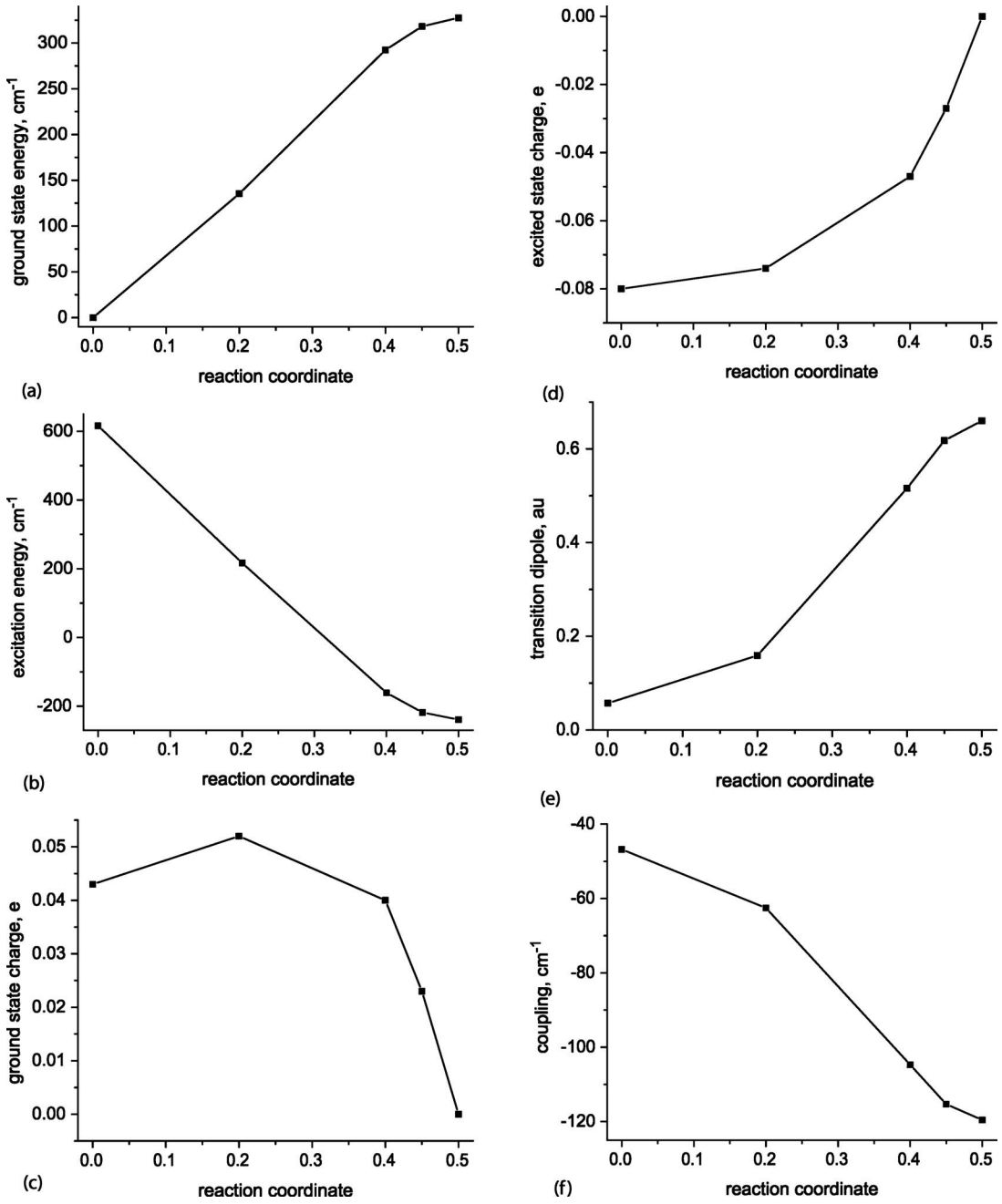

FIG. 10. Error in (a) ground state energy, (b) excitation energy, (c) ground state charge, (d) excited state charge, (e) transition dipole moment, and (f) diabatic coupling in $(LiH)_2^+$. EOM-IP-CCSD/6-31+G results are shown.

and 1.329 Å, respectively. The vertical EOM-IP-CCSD/6-31+G IE of ethylene fragment at neutral geometry is 10.381 eV, while that at the cation geometry is 10.049 eV. We chose the parallel stacked geometry in which the planes of the molecules are separated by 4.0 and 6.0 Å. The results are in Table IX and Figs. 11 and 12.

Figure 11 presents the ground state PES and the charge distribution along the CT reaction coordinate in the ethylene dimer cation at 4 and 6 Å separations. EOM-IP-CCSD produces a smooth change in both quantities, whereas the CCSD curve (using doublet reference) exhibits a cusp at $R=0.5$. Note that the cusp is present for both UHF and ROHF based curves and is due to unbalanced description of the important electronic configurations by doublet-reference based CCSD rather than spin contamination of the reference.

Since this system is beyond the reach of FCI, we compare the EOM-IP-CCSD and CCSD/EE-CCSD results against more accurate EOM-IP-CC(2,3) (EOM-IP-CCSD/$3h2p$) values, as well as MR-CISD+Q. As expected, EOM-IP-CC(2,3) and MR-CISD+Q are in an excellent agreement. Both methods predict a deeper potential well, the difference being ~ 100 cm^{-1}. MR-CISD+Q curve has a small cusp due to the frozen core, e.g., the cusp disappears if the excitations from core orbitals are included at MR-CISD level. Unfortunately, it was not possible to simultaneously unfreeze the core and employ adequately large active space in MRCI calculations.

Overall, EOM-IP-CCSD, EOM-IP-CC(2,3), and MR-CISD predict very similar, smooth changes of the fragment

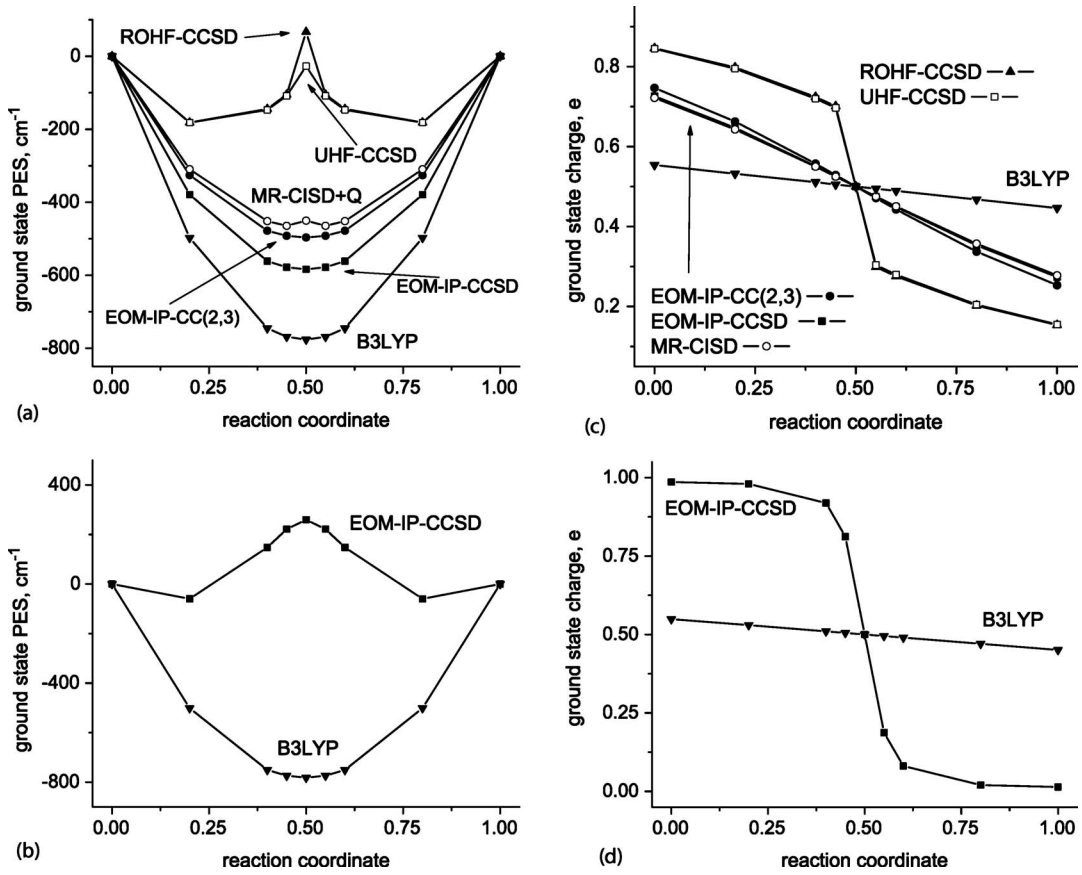

FIG. 11. Changes in charge distribution and PES scans along the CT coordinate in the ground state of $(C_2H_4)_2^+$ at 4 Å [panels (a) and (c)] and 6 Å separations [panels (b) and (d)].

charge. The degree of charge localization is exaggerated in CCSD calculation. This causes an unphysically abrupt change in the polarity of the system around the transition state. Similar discrepancy between EOM-IP-CCSD and EOM-EE-CCSD is present in the excited state (not shown).

DFT/B3LYP calculation yields qualitatively correct shapes of the PES at 4 Å; however, the depth and the degree of charge delocalization are severely overestimated, due to SIE. As the distance between the fragments increases, the $R=0.5$ point would become a transition state separating to charge-localized minima. At the EOM-IP-CCSD level, this happens at 6 Å, whereas B3LYP still predicts a potential well and significant charge delocalization. In fact, there is only a minor change between the B3LYP results at 4 and 6 Å. Of course, SIE-corrected functionals, e.g., long-range corrected functionals,[105,106] should be able to better describe these CT systems.

Since the density matrices at the EOM-IP-CC(2,3) level are not available, we have restricted ourselves to the calculation of energies and permanent dipoles via finite differences. All differences shown in Fig. 12 were calculated relative to EOM-IP-CC(2,3).

As is evident from Fig. 12(a), the depth of the potential well along R is overestimated by EOM-IP-CCSD. The largest error is 80 cm^{-1} and occurs at $R=0.5$. This is best compared to the excitation energy, which at this point is 4603 cm^{-1}. The MR-CISD+Q/EOM-IP-CC(2,3) difference is approximately half of the EOM-IP-CCSD error. The error in the excitation energy is shown in Fig. 12(b). For EOM-IP-CCSD it decreases toward the transition state from 200 to 50 cm^{-1}. In other words, the quality of the EOM-IP-CCSD wave function improves as the monomers become more similar; however, NPE is appreciable. Figures 12(c) and 12(d) show the ground and excited state charge. In both cases, the EOM-IP-CCSD and MR-CISD methods underpolarize the CT state relative to EOM-IP-CC(2,3). The magnitude of the difference is small, thus yielding credence to the transition dipole moment. As seen previously, exaggerated delocalization leads to transition dipole moments that are typically too high. The diabatic coupling varies smoothly with R (not shown). The lack of EOM-IP-CC(2,3) transition dipole prevents us from making a direct comparison of the diabatic coupling. In other systems studied we have witnessed a peculiar error cancellation between ingredients of Eq. (5), which gives us confidence in the presented values. A comparison between MRCI and EOM-IP-CCSD is very interesting. Quantitatively the results are very similar. Note, however, that while EOM-IP-CCSD coupling changes by 2 cm^{-1} between $R=0$ and $R=0.5$, MRCI predicts a 90 cm^{-1} change.

IV. CONCLUSIONS

The presented results demonstrate that EOM-IP-CCSD is a reliable method for the study of noncovalent ionized dimers. It yields smooth variation of energies and molecular

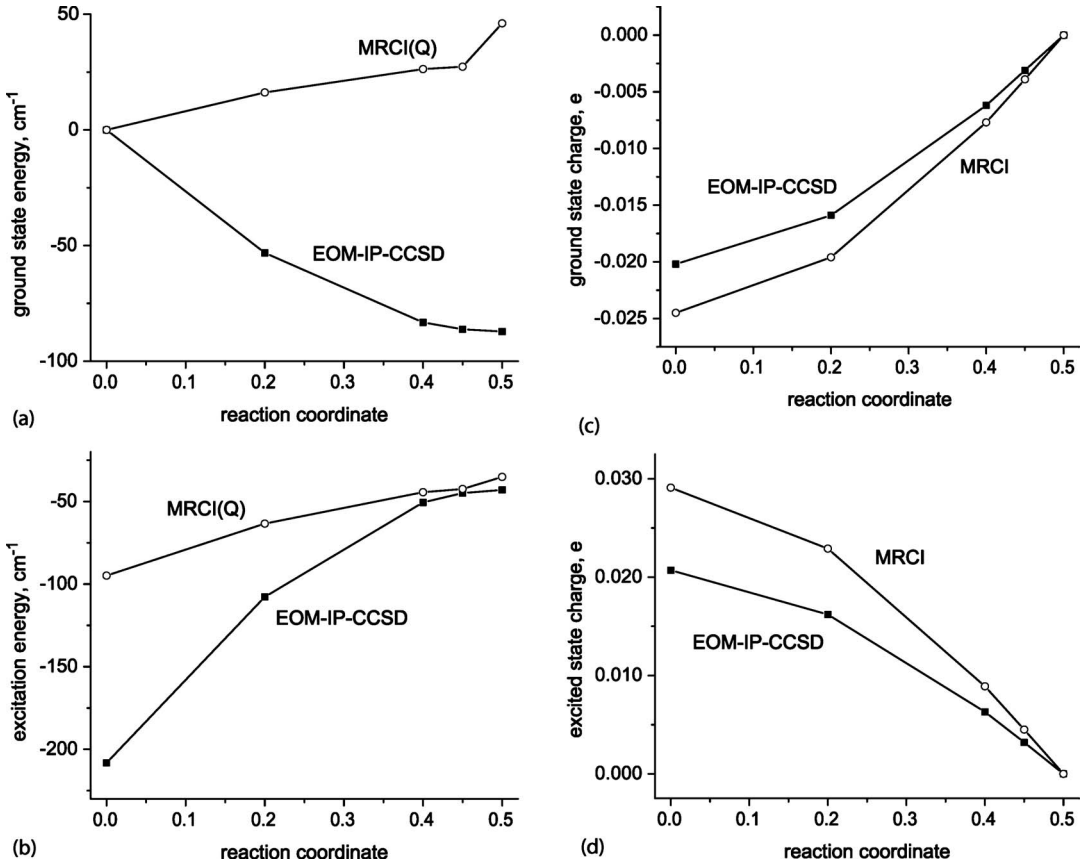

FIG. 12. Differences against EOM-IP-CCSD($3h2p$) for (a) ground state energy, (b) excitation energy, (c) ground state charge, and (d) excited state charge in $(C_2H_4)_2^+$.

properties with nuclear coordinates. Most importantly, the cusp in the PES along charge transfer coordinates that is associated with the open-shell reference is completely avoided. Also, the NPE is typically small. In other words, different spatial arrangements of the fragments are described with equal accuracy. The advantages of the EOM-IP method become even more important when the ionized states of the monomers feature electronic degeneracies, as in benzene dimer cation.[8]

In cases where the difference in IEs is much larger than the coupling, EOM-IP-CCSD and EOM-EE-CCSD perform similarly. Due to the lower computational scaling, the former method is preferable. An argument can be made that just like EOM-EE-CCSD overpolarizes the states, the EOM-IP-CCSD method may appreciably underpolarize the states. In the studied systems only a small degree of underpolarization has been observed. The diabatic coupling has proved to be a fairly insensitive probe of the quality of state description. The increased polarity of EOM-EE-CCSD states is offset by lower transition dipoles and higher excitation energies. Comparison of transition dipole moments offers a better one-number descriptor of the quality of the ground and excited state wave functions.

We expect that the presented results will provide useful calibration data for calculation of electronic coupling elements as well as dimer properties.

ACKNOWLEDGMENTS

This work was conducted in the framework of the Center for Computational Studies of Electronic Structure and Spectroscopy of Open-Shell and Electronically Excited Species (iopenshell.usc.edu) supported by the National Science Foundation through the CRIF:CRF CHE-0625419+0624602 +0625237 grant. A.I.K. and S.E.B. also gratefully acknowledge support of the National Science Foundation through the CHE-0616271 and CHE-0617060 grants, respectively. We wish to thank the University of Southern California Center for High Performance Computing and Communications for making their computational resources available and technical support throughout this project. S.A.A. and C.D.S. gratefully acknowledge support from the National Science Foundation through Grant No. CHE-0094088, the Petroleum Research Fund through Grant No. 44262-AC6, and Georgia Tech's Center for Organic Photonics and Electronics (COPE).

[1] M. D. Newton, Chem. Rev. (Washington, D.C.) **91**, 767 (1991).
[2] A. Amini and A. Harriman, J. Photochem. Photobiol. C **4**, 155 (2003).
[3] H. B. Gray and J. R. Winkler, Q. Rev. Biophys. **36**, 341 (2003).
[4] R. G. Endres, D. L. Cox, and R. R. P. Singh, Rev. Mod. Phys. **76**, 195 (2004).
[5] Y. Inokuchi, Y. Naitoh, K. Ohashi, K. Saitow, K. Yoshihara, and N. Nishi, Chem. Phys. Lett. **269**, 298 (1997).
[6] K. Okamoto, A. Saeki, T. Kozawa, Y. Yoshida, and S. Tagawa, Chem. Lett. **2003**, 834 (2003).
[7] K. Enomoto, J. A. LaVerne, and M. S. Araos, J. Phys. Chem. A **111**, 9 (2007).
[8] P. A. Pieniazek, A. I. Krylov, and S. E. Bradforth, J. Chem. Phys. **127**,

044317 (2007).
[9] Y. Achiba, S. Tomoda, and K. Kimura, Chem. Phys. Lett. **87**, 197 (1982).
[10] J. R. Grover, E. A. Walters, and E. T. Hui, J. Phys. Chem. **91**, 3233 (1987).
[11] H. Krause, B. Ernstberger, and H. J. Neusser, Chem. Phys. Lett. **184**, 411 (1991).
[12] G. C. Reid, Adv. At. Mol. Phys. **12**, 375 (1976).
[13] E. E. Ferguson, F. C. Fehsenfield, and D. L. Albritton, in *Gas Phase Ion Chemistry*, edited by M. T. Bowers (Academic, New York, 1979), Vol. 1, pp. 45–82.
[14] R. Lindh and L. A. Barnes, J. Chem. Phys. **100**, 224 (1994).
[15] Y. M. Rhee, T. J. Lee, M. S. Gudipati, L. J. Allamandola, and M. Head-Gordon, Proc. Natl. Acad. Sci. U.S.A. **104**, 5274 (2007).
[16] A. J. Illies, M. L. McKee, and H. B. Schlegel, J. Phys. Chem. **91**, 3489 (1987).
[17] S. P. de Visser, L. J. de Koning, and N. M. M. Nibbering, J. Phys. Chem. **99**, 15444 (1995).
[18] P. C. Hiberty, S. Humbel, D. Danovich, and S. Shaik, J. Am. Chem. Soc. **117**, 9003 (1995).
[19] M. Sodupe, J. Bertran, L. Rodriguez-Santiago, and E. J. Baerends, J. Phys. Chem. A **103**, 166 (1999).
[20] K. Ohashi, Y. Nakai, T. Shibata, and N. Nishi, Laser Chem. **14**, 3 (1994).
[21] I. A. Shkrob, M. C. Sauer, Jr., C. D. Jonah, and K. Takahashi, J. Phys. Chem. A **106**, 11855 (2002).
[22] R. A. Marcus, Discuss. Faraday Soc. **29**, 21 (1960).
[23] R. A. Marcus, J. Chem. Phys. **43**, 679 (1965).
[24] R. A. Marcus and N. Sutin, Biochim. Biophys. Acta **811**, 265 (1985).
[25] J. R. Norris, R. A. Uphaus, H. L. Crespi, and J. Katz, Proc. Natl. Acad. Sci. U.S.A. **68**, 625 (1971).
[26] L. Y. Zhang and R. A. Friesner, Proc. Natl. Acad. Sci. U.S.A. **95**, 13603 (1998).
[27] D. Leys, T. E. Meyer, A. S. Tsapin, K. H. Nealson, M. A. Cusanovich, and J. J. Van Beeumen, J. Biol. Chem. **277**, 35703 (2002).
[28] D. M. A. Smith, K. M. Rosso, M. Valiev, M. Dupuis, and T. P. Straatsma, J. Phys. Chem. B **110**, 15582 (2006).
[29] S. Delaney and J. K. Barton, J. Org. Chem. **68**, 6475 (2003).
[30] E. R. Davidson and W. T. Borden, J. Phys. Chem. **87**, 4783 (1983).
[31] N. J. Russ, T. D. Crawford, and G. S. Tschumper, J. Chem. Phys. **120**, 7298 (2005).
[32] L. Rodriguez-Monge and S. Larsson, J. Phys. Chem. **100**, 6298 (1996).
[33] R. J. Cave and M. D. Newton, J. Chem. Phys. **106**, 9213 (1997).
[34] C. Carra, N. Iordanova, and S. Hammes-Schiffer, J. Phys. Chem. B **106**, 8415 (2002).
[35] W. Eisfeld and K. Morokuma, J. Chem. Phys. **113**, 5587 (2000).
[36] A. I. Krylov, Chem. Phys. Lett. **338**, 375 (2001).
[37] S. V. Levchenko and A. I. Krylov, J. Chem. Phys. **120**, 175 (2004).
[38] A. I. Krylov, Acc. Chem. Res. **39**, 83 (2006).
[39] Z. Q. You, Y. H. Shao, and C. P. Hsu, Chem. Phys. Lett. **390**, 116 (2004).
[40] P. O. Löwdin, Rev. Mod. Phys. **35**, 496 (1963).
[41] R. D. Cohen and C. D. Sherrill, J. Chem. Phys. **114**, 8257 (2001).
[42] T. Bally and G. N. Sastry, J. Phys. Chem. A **101**, 7923 (1997).
[43] V. Polo, E. Kraka, and D. Cremer, Mol. Phys. **100**, 1771 (2002).
[44] Y. Zhang and W. Yang, J. Chem. Phys. **109**, 2604 (1998).
[45] M. Lundber and P. E. M. Siegbahn, J. Chem. Phys. **122**, 224103 (2005).
[46] A. Dreuw and M. Head-Gordon, Chem. Rev. (Washington, D.C.) **105**, 4009 (2005).
[47] A. Dreuw and M. Head-Gordon, Chem. Phys. Lett. **426**, 231 (2006).
[48] L. V. Slipchenko and A. I. Krylov, J. Phys. Chem. A **110**, 291 (2006).
[49] V. Vanovschi, A. I. Krylov, and P. G. Wenthold, "Structure, vibrational frequencies, ionization energies, and photoelectron spectrum of the para--benzyne radical anion," Theor. Chim. Acta (in press).
[50] D. Sinha, D. Mukhopagedhyay, and D. Mukherjee, Chem. Phys. Lett. **129**, 369 (1986).
[51] S. Pal, M. Rittby, R. J. Bartlett, D. Sinha, and D. Mukherjee, Chem. Phys. Lett. **137**, 273 (1987).
[52] D. Sinha, D. Mukhopadhya, R. Chaudhuri, and D. Mukherjee, Chem. Phys. Lett. **154**, 544 (1989).
[53] R. Chaudhuri, D. Mukhopadhyay, and D. Mukherjee, Chem. Phys. Lett. **162**, 393 (1989).
[54] J. F. Stanton and J. Gauss, J. Chem. Phys. **101**, 8938 (1994).
[55] J. F. Stanton and J. Gauss, J. Chem. Phys. **111**, 8785 (1999).
[56] C. H. Yang and C. P. Hsu, J. Chem. Phys. **124**, 244507 (2006).
[57] J. Simons and W. D. Smith, J. Chem. Phys. **58**, 4899 (1973).
[58] H. Nakatsuji and K. Hirao, J. Chem. Phys. **68**, 2053 (1978).
[59] H. Nakatsuji, Chem. Phys. Lett. **177**, 331 (1991).
[60] R. J. Cave and M. D. Newton, Chem. Phys. Lett. **249**, 15 (1996).
[61] E. J. P. Malar and A. K. Chandra, J. Phys. Chem. **85**, 2190 (1981).
[62] P. Jungwirth and T. Bally, J. Am. Chem. Soc. **115**, 5783 (1993).
[63] See EPAPS Document No. E-JCPSA6-127-306741 for the molecular structures, total energies, as well as transition and permanent dipole moments. This document can be reached through a direct link in the online article's HTML reference section or via the EPAPS homepage (http://www.aip.org/pubservs/epaps.html).
[64] D. J. Rowe, Rev. Mod. Phys. **40**, 153 (1968).
[65] K. Emrich, Nucl. Phys. A **351**, 379 (1981).
[66] H. Sekino and R. J. Bartlett, Int. J. Quantum Chem., Quantum Chem. Symp. **18**, 255 (1984).
[67] J. Geertsen, M. Rittby, and R. J. Bartlett, Chem. Phys. Lett. **164**, 57 (1989).
[68] J. F. Stanton and R. J. Bartlett, J. Chem. Phys. **98**, 7029 (1993).
[69] R. J. Bartlett and J. F. Stanton, Rev. Comput. Chem. **5**, 65 (1994).
[70] R. J. Bartlett, Int. J. Mol. Sci. **3**, 579 (2002). A relation between MR-CC, Fock space, and EOM methods is discussed.
[71] A. I. Krylov, "Equation-of-motion coupled-cluster methods for open-shell and electronically excited species: The hitchhiker's guide to Fock space," Annu. Rev. Phys. Chem. (in press).
[72] J. Olsen, J. Chem. Phys. **113**, 7140 (2000).
[73] H. Koch, H. J. Aa. Jensen, P. Jørgensen, and T. Helgaker, J. Chem. Phys. **93**, 3345 (1990).
[74] L. Meissner and R. J. Bartlett, J. Chem. Phys. **94**, 6670 (1991).
[75] M. Nooijen, K. R. Shamasundar, and D. Mukherjee, Mol. Phys. **103**, 2277 (2005).
[76] J. F. Stanton, J. Chem. Phys. **101**, 8928 (1994).
[77] H. Koch, R. Kobayashi, A. S. de Merás, and P. Jørgensen, J. Chem. Phys. **100**, 4393 (1994).
[78] See, for example, footnote 32 in Ref. 38 explaining size consistency of EOM-EE/SF, as well as related discussion in Ref. 85. In the context of charge transfer systems of a $A^+B \rightarrow AB^+$ type, this means that the EOM-IP ionization energies, PESs, and energy gaps between the PESs will not be affected by any number of closed-shell species at infinite distance. For example, all the EOM-IP results for the ionized ethylene dimer from Sec. III F (except for the total energies) will remain unchanged if we add a neutral ethylene dimer at sufficiently large distance. Therefore, the quality of EOM-IP description does not deteriorate with molecular size increase. However, the lack of full size extensivity means that EOM-IP is not capable of describing *simultaneously* two noninteracting ionized ethylene dimers.
[79] S. A. Kucharski, M. Włoch, M. Musiał, and R. J. Bartlett, J. Chem. Phys. **115**, 8263 (2001).
[80] K. Kowalski and P. Piecuch, J. Chem. Phys. **115**, 643 (2001).
[81] M. Nooijen and R. J. Bartlett, J. Chem. Phys. **102**, 3629 (1995).
[82] S. Hirata, M. Nooijen, and R. J. Bartlett, Chem. Phys. Lett. **328**, 459 (2000).
[83] M. Kamyia and S. Hirata, J. Chem. Phys. **125**, 074111 (2006).
[84] P. Piecuch and R. J. Bartlett, Adv. Quantum Chem. **34**, 295 (1999).
[85] L. V. Slipchenko and A. I. Krylov, J. Chem. Phys. **123**, 84107 (2005).
[86] C. A. Mead and D. G. Truhlar, J. Chem. Phys. **77**, 6090 (1982).
[87] A. Macías and A. Riera, J. Phys. B **11**, L489 (1978).
[88] H.-J. Werner and W. Meyer, J. Chem. Phys. **74**, 5802 (1981).
[89] C. Petrongolo, G. Hirsch, and R. J. Buenker, Mol. Phys. **70**, 825 (1990).
[90] M. H. Alexander, J. Chem. Phys. **99**, 6014 (1993).
[91] A. J. Dobbyn and P. J. Knowles, Mol. Phys. **91**, 1107 (1997).
[92] D. R. Yarkony, J. Phys. Chem. A **102**, 8073 (1998).
[93] Y. Shao, L. F. Molnar, Y. Jung, *et al.*, Phys. Chem. Chem. Phys. **8**, 3172 (2006).
[94] T. D. Crawford, C. D. Sherrill, E. F. Valeev, J. T. Fermann, R. A. King, M. L. Leininger, S. T. Brown, C. L. Janssen, E. T. Seidl, J. P. Kenny, and W. D. Allen, J. Comput. Chem. **28**, 1610 (2007).
[95] H.-J. Werner, P. J. Knowles, R. Lindh *et al.*, MOLPRO 2002.6, 2003.
[96] Basis sets were obtained from the Extensible Computational Chemistry Environment Basis Set Database, Version, as developed and distributed by the Molecular Science Computing Facility, Environmental and Molecular Sciences Laboratory which is part of the Pacific Northwest Laboratory, P.O. Box 999, Richland, Washington 99352, and funded by the U.S. Department of Energy. The Pacific Northwest Laboratory is a multiprogram laboratory operated by Battelle Memorial Institue for the U. S. Department of Energy under Contract No. DE-AC06-76RLO 1830. Contact David Feller or Karen Schuchardt for further information.

[97] S. V. Levchenko, T. Wang, and A. I. Krylov, J. Chem. Phys. **122**, 224106 (2005).
[98] P. J. Bruna and S. D. Peyerimhoff, *Ab initio Methods in Quantum Chemistry* (Wiley, New York, 1987), Vol. 1, pp. 1–98.
[99] H. J. Werner and P. J. Knowles, J. Chem. Phys. **89**, 5803 (1988).
[100] S. R. Langhoff and E. R. Davidson, Int. J. Quantum Chem. **8**, 61 (1974).
[101] K. Raghavachari, G. W. Trucks, J. A. Pople, and M. Head-Gordon, Chem. Phys. Lett. **157**, 479 (1989).
[102] J. D. Watts, J. Gauss, and R. J. Bartlett, J. Chem. Phys. **98**, 8718 (1993).
[103] A. D. Becke, J. Chem. Phys. **98**, 5648 (1993).
[104] A. I. Krylov, C. D. Sherrill, E. F. C. Byrd, and M. Head-Gordon, J. Chem. Phys. **109**, 10669 (1998).
[105] T. Tsuneda, M. Kamiya, and K. Hirao, J. Comput. Chem. **24**, 1592 (2003).
[106] Y. Tawada, T. Tsuneda, S. Yanagisawa, T. Yanai, and K. Hirao, J. Chem. Phys. **120**, 8425 (2004).